Electrochemical Aspects of STM and Related Techniques

P. A. Christensen

The Chemistry Department, Bedson Building, The University, Newcastle upon Tyne NE1 7RU

1 Introduction

The importance of acquiring a detailed understanding of the solid/liquid interface has long been recognized with respect to its role in catalysis and electrochemistry. This interest has resulted in an explosion in the number and variety of surface analytical techniques, both *in situ* and *ex situ*, over the past twenty years. More particularly, the past decade has seen the increasingly routine application of *in situ* infrared, Raman, EPR, and, *X*-ray spectroscopies, ellipsometry, *etc.*[1,2] These techniques have proved to be extremely valuable in helping to elucidate the complex processes that occur at the electrode/electrolyte interface even though they can only provide information averaged over the electrode surface. In contrast, it is widely accepted that a high proportion of the chemical or electrochemical phenomena that take place at solid surfaces do so at 'active sites': defects, adatoms, kinks, or particular arrangements of a few atoms. Whilst there are techniques, such as electron bombardment methods, capable of providing structural information on such sites, down to *ca.* 30—50 Å resolution, they require Ultra High Vacuum conditions to operate; and the application of emersion techniques carries with it the possibility of, for example, surface reconstruction during the transfer between the electrochemical cell and the UHV chamber. The advent of Scanning Tunnelling Microscopy (STM) filled a major gap in the surface scientist's armoury and was rapidly seized upon by electrochemists eager to exploit its unique capability of providing *real space* images of the surface of a conducting sample with *atomic resolution*.

The technique of STM was first reported by Binnig, Rohrer, and colleagues in the early eighties.[3] STM relies upon quantum-mechanical tunnelling of electrons between a sharp tip and a conducting sample, maintained by the presence of a potential difference between the two, to obtain an atomic resolution 'picture' of the sample surface. Topographical images of the surface are obtained by monitoring the tip–sample distance (at constant tunnelling current) or the magnitude of the tunnelling current (at fixed tip–sample distance) as the tip is drawn across the sample.

Under UHV conditions, STM has a lateral resolution (*i.e.* parallel to the surface) of *ca.* 5 Å, and a vertical resolution of 0.1 Å; the impact of a structural technique having such a resolution can best be conveyed in a picture. Thus, Figure 1 shows an STM image of the surface of Highly Ordered Pyrolytic Graphite, (HOPG), obtained by Cataldi and Briggs.[4] The *individual atoms* can clearly be seen.

At first sight, STM might be thought to be limited to the study of surfaces under UHV conditions, but STM has had a major impact on electrochemistry, and continues to provide exciting insights into the atomic-scale processes responsible for the phenomena we usually measure.

Dr. Paul Christensen was educated at South Shields Grammar School and Exeter College, Oxford. He carried out the research towards his Ph.D. at the Royal Institution under the supervision of Lord Porter. Dr. Christensen has been a Lecturer in Physical Chemistry at Newcastle University since October 1989, and his research interest lies primarily in the use of in-situ techniques such as STM, FTIR, Ellipsometry etc. to study the electrode/electrolyte interface.

This paper is not intended to be an exhaustive review of electrochemical STM, or related techniques; there are many excellent such reviews in the literature, (see, for example, references 5 and 6). Instead, it is intended to provide an introduction to STM, Scanning Tunnelling Spectroscopy, and Atom Force Microscopy, with particular respect to their strengths and weaknesses when applied *in situ* in electrochemistry.

2 Scanning Tunnelling Microscopy

2.1 Mechanics

As was mentioned above, the essence of STM lies in the quantum-mechanical tunnelling of electrons between a sharp metal tip and the surface of a *conducting* substrate, maintained by a bias potential between the two; tunnelling occurs when the wavefunctions of the tip and sample overlap. Thus, the tip is first brought near the sample *via* a coarse *z* positioner, such as a 10:1 reducing lever, or a controlled-approach piezo-electric motor, (Inchworm™). The latter provides a 10 Å step size, and a movement of up to 0.5 mm s^{-1}. As soon as tunnelling current is detected, the tip is stopped, and the fine control system switched in. Thus, the actual STM tip is suspended over the sample surface by a piezo-electric mount that consists of either three linear crystals arranged orthogonally, or a single crystal 'tube' scanner; in either case allowing movement in the *x*,*y*, and *z* directions, see Figures 2a and b. This system takes over the cautious advance of the tip until the desired tunnelling current is achieved, usually corresponding to a tip–sample separation of *ca.* 5—10 Å, and then is used to raster the tip across the surface and obtain the image. The data collection is generally performed in one of two ways:

2.1.1 Constant Current

The tip is moved along a fixed trajectory in the *x* direction, and the tunnelling current, i_t, monitored. A feedback loop is then used to move the tip up or down in order to maintain a constant current, (see Figure 3a). At the end of a single scan, the tip is displaced a single step in the *y*-direction, and the scan repeated; the image obtained is thus a linescan plot of (*x*,*y*,*z*). The imaging speed is severely limited by the response time of the feedback loop and *z* piezo; too fast and the tip risks crashing into an atomic mountain, a typical scan rate is < 5000 Å s^{-1}.

2.1.2 Constant Height

In this approach, the tip–sample distance is fixed during the scan, and the variation in tunnelling current is plotted as a function of lateral position, see Figure 3b. Thus, only the electronics have to respond, rather than the piezoelectric crystal. As a result, the imaging speed can be increased, by a factor of up to two orders of magnitude. The constant height method can only be used to image very flat areas of the sample, and requires the relationship between i_t and the tip–sample separation if images of the sample surface are to be obtained in terms of the *z* displacement. This is usually achieved by calibration with a surface of known geometry.

Images from both methods are in the form of line scans; image enhancement procedures may then be employed to convert the raw data into grey-scale or colour images.

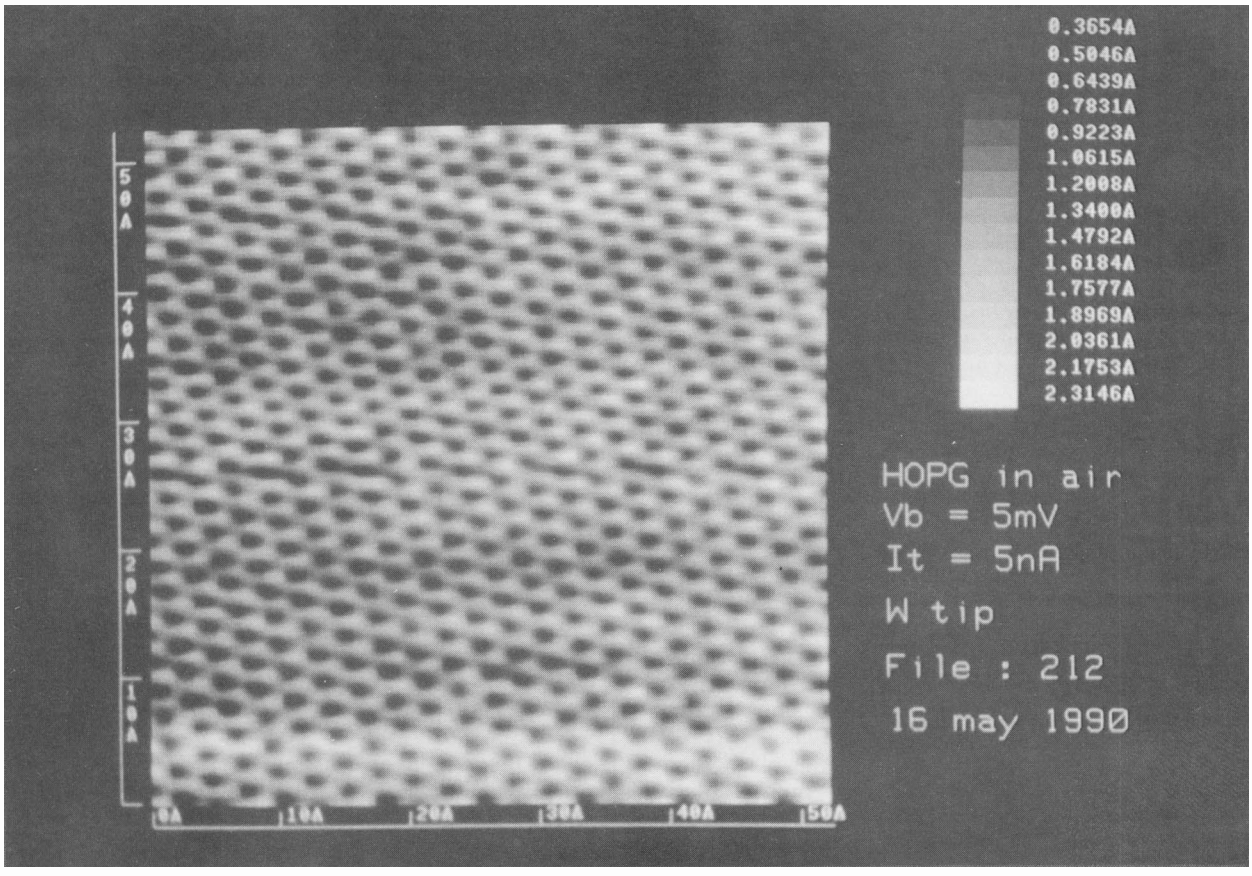

Figure 1 STM image of HOPG in air. Tungsten tip, bias voltage 5 mV, tunnelling current 5 nA.
(Reproduced with permission from Dr. G. A. D. Briggs.)

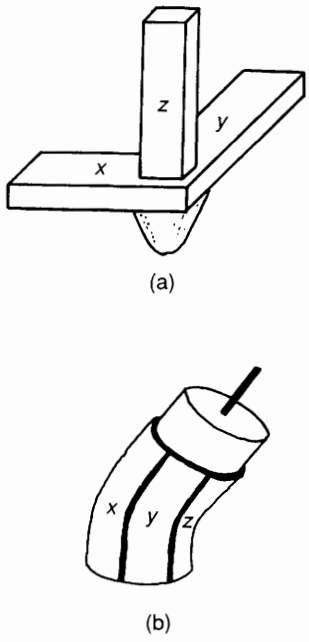

Figure 2 Schematic representations of (a) three-way piezo-electric scanner and (b) a tube scanner.

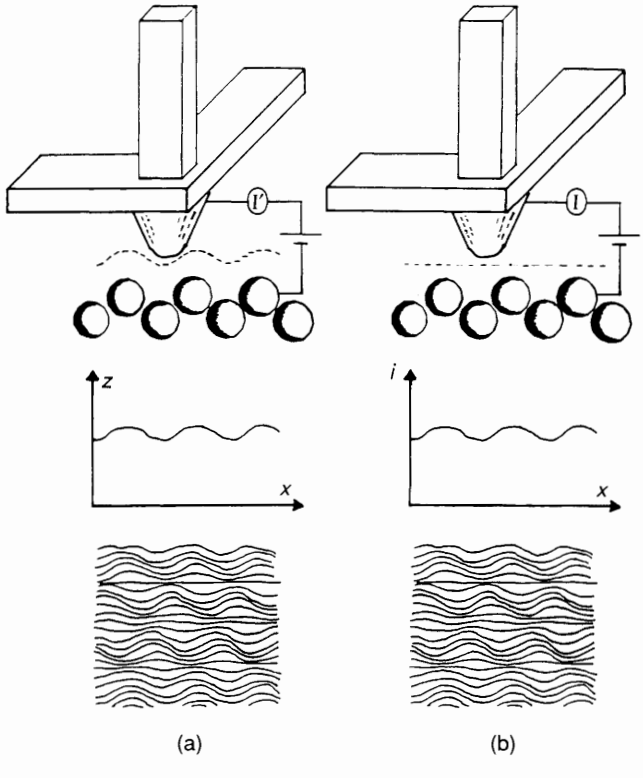

Figure 3 Schematic representation of the (a) constant current, and (b) constant height modes of operation of an STM.

2.2 Principles

The basis of all tunnelling microscopies is electron tunnelling through a potential barrier. This process has no chemical analogy, and it is most easily understood by considering the progress of a free electron wave from left to right in Figure 4a. For simplicity, we will only consider tunnelling between metals.

In regions I and III the electron has zero potential energy, all of its energy is kinetic. In region II, the electron experiences a potential U_0, over a region from $z = 0$ to $z = d$.

In regions I and III, the Schrödinger equation for the electron takes the simple form:

$$[-\hbar^2/2m_e].d^2\Psi/dz^2 = E\Psi \tag{1}$$

where m_e is the mass of the electron, and E is the energy as shown in the figure. This can be solved immediately to give, in region I:

$$\Psi_I = Ae^{ikz} + Be^{-ikz} \tag{2}$$

where $k = [2m_eE/\hbar^2]^{1/2}$, A and B are constants, and the momentum of the electron is just $\hbar k$. The first term represents the electron transition from left to right; the second allows for interference between the incident wave and the wave corresponding to *reflection* from the barrier. Evidently, in region III:

$$\Psi_{III} = Fe^{ikz} \tag{3}$$

where F is a constant, since only the transmitted wave is of interest.

In region II, by contrast, the appropriate form of the Schrödinger equation is:

$$[\hbar^2/2m_e]d^2\Psi/dz^2 = [U_0 + E] \tag{4}$$

and provided $U_0 > E$, has the solution:

$$\Psi_{II} = Ce^{k'z} + De^{-k'z} \tag{5}$$

where $k' = [2m_e(U_0 + E)/\hbar^2]^{1/2}$

The dominant term, save close to the II/III boundary, is the second, and physically this corresponds to the *exponential decay* of the wavefunction as the barrier is traversed. This is a remarkable result: classically, we would expect the electron to be completely reflected at the I/II interface, but quantum mechanics shows that this will not happen unless $U_0 \to \infty$. At finite values of U_0, the wavefunction decays exponentially into the barrier, with $|\Psi|^2 \approx e^{-2k'z}$. It is instructional to evaluate k': for $E = 2$ eV and $U_0 = 6$ eV, we have $k' = 10^{10}$ m^{-1}. Hence, $|\Psi_{II}|^2$ *decays by a factor of ca. 7 for every 1 Å thickness of the barrier.*

The tunnelling probability, $P_T(E)$, through the rectangular barrier of Figure 4a can be obtained approximately by calculating the total decay in the wavefunction over the entire barrier. This is clearly given by:

$$P_T(E) = e^{-2k'd} \tag{6}$$

where d is the sample–tip separation. If the barrier is *not* rectangular, and the potential energy is now a function of z, then it can be readily shown that:

$$P_T(E) = \exp\{-2\int_{z_l}^{z_r} [2m_e\{U(z) + E\}/\hbar^2]^{\frac{1}{2}}dz\} \tag{7}$$

which is termed the WKB approximation, and z_l and z_r are the classical turning points, *i.e.* the values of z on the left and right of the barrier for which $U(z) = E$. For a trapezoidal barrier, of the type shown in Figure 4b, we can replace z_l and z_r by 0 and d, respectively. Figure 4b represents the form of Figure 4a for the tip and sample in an STM, with the tip and sample at equilibrium, *i.e.* joined only by a wire. Figure 4c represents the case when the sample is made positive with respect to the tip: *i.e.* a bias potential of V_b is applied, where $V_b = V_{sample} - V_{tip}$. Under these conditions, tunnelling occurs from tip to sample, as shown.

At low bias voltages, such as those typically employed in an STM experiment (*i.e.* for the case given, of tunnelling from tip to sample, $0 < V_b < 0.6$ V), the tunnelling current is given by:

$$i_t \sim [D_s(E_{F,s})D_t(E_{F,t})V_b e^{-2k'd}], \tag{8}$$

Where $D_s(E_{F,s})$ and $D_t(E_{F,t})$ are the density of states *at the Fermi level* of the sample and tip, respectively. Thus, at a fixed (positive) bias, tunnelling is from filled states near the Fermi level of the tip, to empty states on the sample. $D_t(E_{F,t})$ and $D_s(E_{F,s})$ are constant, and the tunnelling current is effectively a function only of the tip–sample separation.

This correlation between i_t and topography breaks down when the surface is not electronically homogenous, *e.g.* when adsorbed species are present, or the sample is a semiconductor. This gives rise to spatially-dependent Local Density Of States, LDOS, and hence $D_s(E_{F,s})$ shows a strong spatial distribution. Thus, a more correct representation of Figure 4c is as shown in Figure 4e; the particular LDOS depicted in the figure will only be true at the particular position of the tip over the surface of the sample.

Figure 5 shows a schematic representation of the tip and sample in an STM experiment. A typical tip diameter is *ca.* 1μm, consequently, if the figure was drawn to the scale of the 'atoms' on the surface, the tip would *ca.* be 10 metres in diameter. Clearly, if the situation was as depicted in Figure 5, the STM would not be capable of atomic resolution. The reason it is lies in the exponential dependence of the tunnelling current on the sample–tip separation, as given in equation 8. Hence, it is thought that tunnelling occurs *via* the selection of one or two atoms lying proud of the mean surface of the tip. Providing that d is large compared to k'^{-1}, then tunnelling occurs from this same atom, or atoms, irrespective of the lateral position of the tip above the surface; the tip density of states can thus be considered as constant. In general, $k' \approx 1$ Å^{-1} whilst $d > 5$ Å. If $d \leqslant 1$ Å, then the precise definition of 'd' is lost, and the tip LDOS show a dependence upon tip position.

Thus the vertical resolution of STM is *ca.* 0.1 Å; the lateral resolution is set by the intersection of the solid cone of current with the surface, and is typically 4—7 Å.[7]

The above empirical treatment really only applies to experiments performed in a vacuum, with no account taken of the effect of placing an electrolyte solution above the sample. Soon after the publication of the initial reports on STM, some controversy existed amongst (increasingly interested) electrochemists as to whether or not the technique would function when tip and sample were immersed in even a weak electrolyte. The concern was that ions of opposite charge from the tip would cluster around it, under the influence of the large electric fields across such a sharp point, perhaps providing numerous tunnelling pathways to degrade the lateral resolution. This was not found to be the case; one explanation given was that electrolytes are ionic conductors but electronic insulators. However, the presence of the electrolyte does have an, as yet unquantified, effect upon the images obtained. Thus, discrepancies have been observed between images obtained under UHV conditions, and those obtained in the presence of electrolyte.[8] It is only recently that workers such as Sass and colleagues[9] have started systematically to investigate the effect upon the tunnelling barrier height, and shape, of the intricate interactions between electrons and a dense ensemble of polar molecules. One approach to such questions, suggested by these workers, is that the trajectory of the tunnelling electrons is not simply described by a solid cone between tip and sample. Instead, the orientational relaxation of particular solvent molecules, or clusters of molecules, may open up particular lower energy routes between tip and sample. These relaxation times will vary with the solvent, and may determine the variation in lateral resolution when the tip-sample spacing is changed. It is clear that our understanding of the physics of

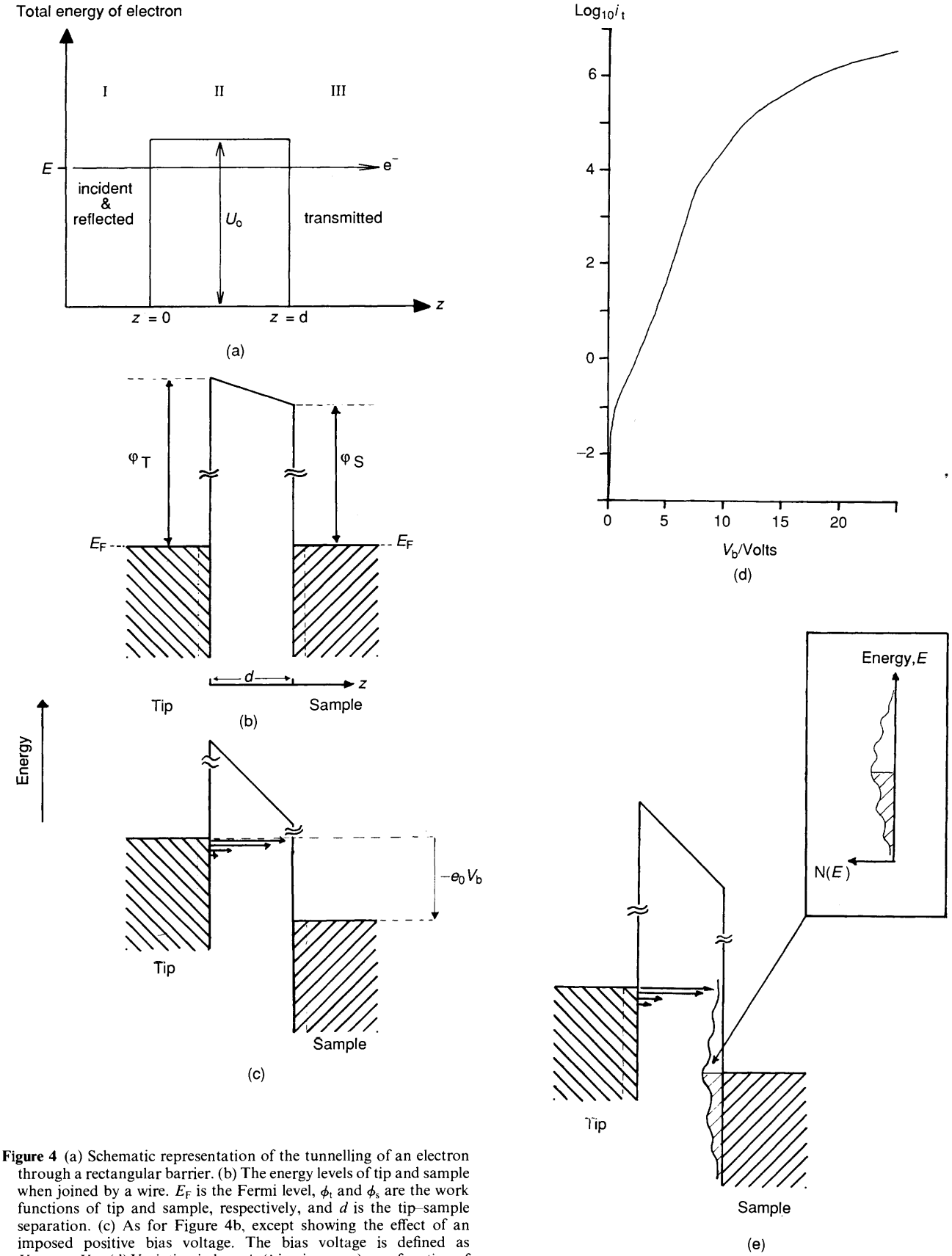

Figure 4 (a) Schematic representation of the tunnelling of an electron through a rectangular barrier. (b) The energy levels of tip and sample when joined by a wire. E_F is the Fermi level, ϕ_t and ϕ_s are the work functions of tip and sample, respectively, and d is the tip–sample separation. (c) As for Figure 4b, except showing the effect of an imposed positive bias voltage. The bias voltage is defined as $V_{sample} - V_{tip}$. (d) Variation in $\log_{10} i_t$, (i_t in picoamps), as a function of bias voltage, calculated on the basis of the principles in equation 8. (After C. R. Leavens and G. C. Aers in reference 7*b*, p. 32). (e) Schematic representation of the energy levels of tip and sample, when sample shows some spatially-dependent Local Density Of States, LDOS.

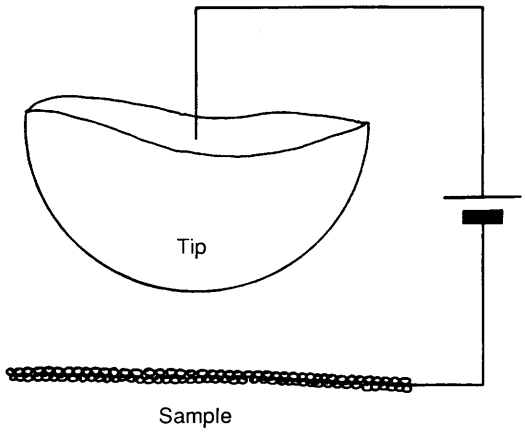

Figure 5 Schematic representation of the STM tip and sample.

electron tunnelling across a liquid gap, particularly for polar solvents, is still incomplete, as is our ability to interpret correctly the images obtained from *in situ* STM. However, for the purposes of this article, the treatment given above is sufficient.

2.3 Practicalities

2.3.1 Tips

Tips, typically Pt/Ir, Au, W, or Ta, are sharpened, either simply by fracture or *via* electrochemical etching. One such method involves forming a 'soap bubble' of 2M NaOH within a Pt/Ir loop, and inserting a length of tungsten tip wire. An a.c. potential of *ca.* 1—15 V peak-to-peak is then applied between tip and loop, at a frequency of 50 Hz. The wire is etched until breaking point, at which time the weight of the wire helps to pull it out into a very fine point.

2.3.2 Samples

The samples should be as flat as possible, if atomic resolution images are required, otherwise a great deal of time is lost searching for atomically flat areas; common samples include Pt or Au evaporated or sputtered onto glass or mica. Layered materials such as Highly Ordered Pyrolytic Graphite, (HOPG), or MoS_2 can be cleaved to reveal fresh, clean surfaces simply by placing sellotape onto the old surface and peeling it away.

2.3.3 Piezo-electric Crystals

The original STM instruments employed three orthogonal piezo elements, one to control scanning in each direction, (see Figure 2a). The device favoured more recently is the tube scanner, as shown in Figure 2b. This still allows fine control in all three directions, but consists of only a single unit.

2.3.4 Cleanliness

An essential practical point is to keep the sample clean, *i.e.* protected from airborne contamination, since adsorption can cause noise on the tunnelling current, as well causing the surface to reconstruct. One way to maintain a clean surface is to hold it in a UHV chamber, the other is to cover it with a highly purified liquid, the latter indicating a possible advantage of operating *in situ*. However, a common contaminant of aqueous electrolyte is Cl^-. Even very low concentrations of chloride ion have been shown to increase substantially the mobility of noble metal ions at anodic potentials, giving rise to an unstable surface. As a result, great care must be exercised when employing a SCE reference electrode to prevent leakage of the Cl^- electrolyte from the reference into the cell.

2.3.5 Potentiostatic Control of the Sample

For STM experiments performed *in vacuo*, it is sufficient simply to apply a bias voltage across the tip and sample in order to obtain tunnelling; and this approach was also employed by Sonnenfeld and Hansma[10] in their early experiments intended to show that STM images could be obtained with a layer of electrolyte above the sample. However, in these experiments, the potential of the sample is undefined with respect to any fixed reference, an unsatisfactory scenario for an electrochemist. Electrochemical control of a sample is usually provided *via* a three-electrode potentiostat and the potential of the sample or working electrode is maintained and monitored very precisely with respect to a non-current carrying reference electrode. Faradaic current flows only between the working and counter electrodes, the latter being usually a Pt loop or gauze. Providing such potentiostatic control of the sample, as well as maintaining a fixed bias potential between sample and tip, is a tricky problem. The essence of this problem is that V_b must be held constant when the sample potential is changed, otherwise spectroscopic information becomes mixed in with the topographic data (see section on Scanning Tunnelling Spectroscopy). Thus, on stepping the sample potential, E_s, prior to collecting an image, then the tip potential E_t must also be changed so as to maintain a constant V_b. Most of the *in situ* electrochemical experiments reported of late (see, for example, references 11—15) employ independent control of E_t and E_s with respect to the reference electrode. The two most popular methods in this respect are:

A three-electrode potentiostat employing a current-carrying reference electrode. Such a reference can support the passage of small currents without altering its potential. The tip acts as a fourth electrode held either at a constant potential with respect to the reference, or at a constant bias voltage with respect to the sample.

Bipotentiostatic control. In effect, the tip and the sample are controlled as two separate and independent working electrodes: this allows true independent control of E_t and E_s with respect to a non-current carrying reference electrode.

In both of the above methods, the bias voltage is given by

$$V_b = E_T - E_s \tag{9}$$

2.3.6 Noise

There are four principal sources of noise in STM:

Imposed vibrations. The tip–sample separation must be stabilized on the sub-Å scale. Hence, the system must be isolated from any external vibrations, particularly those of the building itself. The first STM system achieved this by levitating the entire UHV arrangement on superconducting magnets. Over the few years since, it has been found that much simpler (and cheaper) methods can be just as effective. Thus, a common arrangement used to isolate the STM from vibration is shown in Figure 6. The STM 'head', including the inchworm/tube scanner/tip mount assembly and electrochemical cell, sit upon four or five heavy metal plates; the plates are separated by halved rubber 'O' ring dampers. The vibrational mismatch between each plate/damper pair gives a total reduction in vibration of at least three orders of magnitude. The whole instrument is then suspended *via* four elasticated ropes from the ceiling, or from a suitable frame. In order to prevent acoustic noise, the instrument is covered with a bell jar; this arrangement also allows for some degree of environmental control.

Electronic noise. Careful shielding of the electronics is required, including placing the STM in a Faraday cage.

Thermal drift and piezo-electric creep. These effects render it essential that images are collected quickly, *e.g.* in *ca.* $\leqslant 10$ seconds.

Uncontrolled Faradaic reactions at the tip. These are a potentially major source of noise in electrochemical STM, and to avoid such complications, the potential of the tip should be maintained within the double-layer region (the region of constant current in Figure 7) wherever possible. However, even if the tip potential

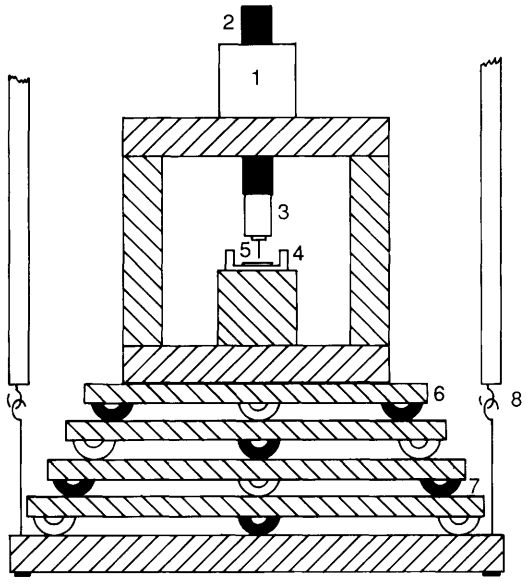

Figure 6 Schematic representation of the STM head and electrochemical cell assembly. (1) Inchworm motor, (2) Inchworm, (3) Faraday cage shield around tube scanner, (4) Teflon pot electrochemical cell, (5) working electrode sample, (6) stainless steel plates, (7) halved Viton 'O' rings, (8) elasticated ropes attached to baseplate. The counter and reference electrodes, and the electrical connection to the sample, are not shown for clarity.

can be maintained in its double layer region, Faradaic reactions can still occur, and it is thus essential that the tip wire be insulated up to as near to the tip itself as possible, in order to minimize the available area accessible to the electrolyte. The insulating materials that have been employed include nail varnish, as well as various waxes.

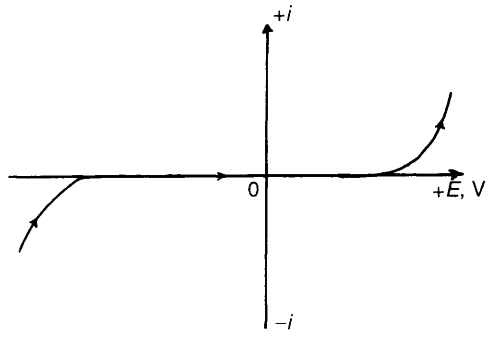

Figure 7 Typical electrochemical response of an STM tip. The Faradaic current flowing in the cathodic region is due to H_2 evolution and the anodic current is due to O_2 evolution or tip dissolution.

Once it was realised that STM could be performed *in situ* in an electrochemical environment, the technique was seized upon by electrochemists who rapidly developed the necessary sophisticated potentiostatic control, and proceeded to produce increasingly exciting and elegant work[5,6] [references 11—15 and references therein]. An example of the potential of STM to provide a causal link between observed electrochemistry and the topographical behaviour of the surface at the atomic level is the work of Itaya, Sugawara, Sashikata, and Furuya[15] which is now described.

2.3.7 The Potential-Dependent Reorganization of Pt(111)

The report by Itaya and colleagues concerns the application of STM to study the effects of potential cycling on the topography of a Pt(111) electrode, and follows the general interest over recent years in the study of well-defined highly-ordered crystals, and of platinum in particular because of its fundamental technological importance as the foremost electrocatalyst. Polycrystalline surfaces are too complicated for such studies, whereas the well-defined, homogeneous, and essentially flat nature of a single-crystal surface provides a readily-understood starting point. An important observation which links single-crystal Pt(111) electrochemistry with that of the polycrystalline material, arises from cyclic voltammetry. Cyclic voltammetry involves the repeated linear ramping of the potential of the sample electrode between two preset limits and simultaneously monitoring the current that passes. If Pt(111) is cycled in this manner between a potential above that at which hydrogen evolution takes place and one in the double layer region, as shown in Figure 8a, then the surface is stable; the various features in the voltammogram merely indicate the formation and removal of surface hydrides. However, if the electrode is cycled up to a potential where surface oxides are formed, and back, then the cyclic voltammogram is observed to revert rapidly to that expected for polycrystalline Pt, see Figure 8b.

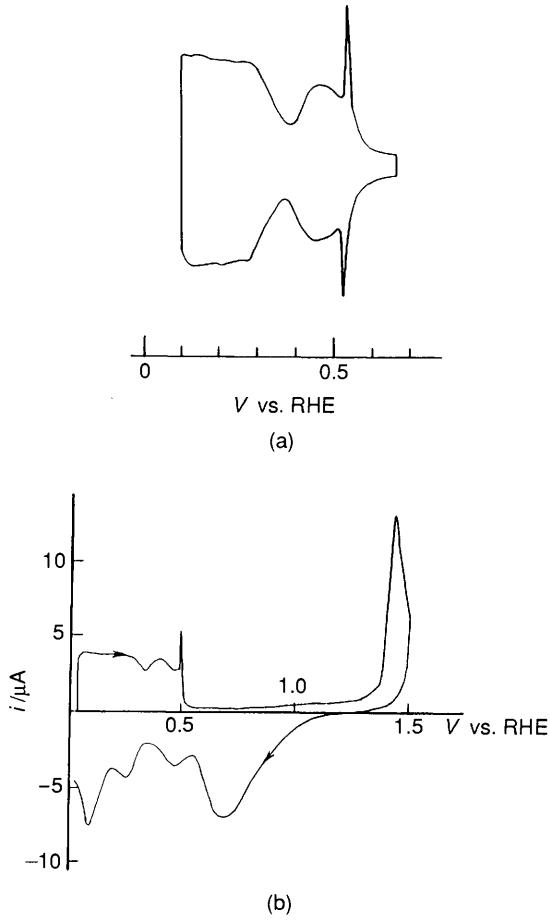

Figure 8 Cyclic voltammograms for a Pt(111) electrode immersed in 0.05 M H_2SO_4. (a) 0.1 V to 0.65 V *versus* the Reversible Hydrogen Electrode, (RHE); (b) 0.05 V to 1.5 V *versus* RHE.

Itaya and colleagues decided to employ STM to see if any correlation existed between the surface topography and the electrochemistry in Figures 8a and b. The images were obtained at constant current, with the tip and sample controlled independently.

Figure 9 shows a token STM image of a 1000 Å × 1000 Å area of the Pt(111) surface. The image was collected at 0.95 V *versus* the Reversible Hydrogen Electrode, RHE, *i.e.* in the double layer region, (see Figures 8a and b). As can be seen, the surface is

dominated by steps of *ca.* 2.3 Å, consistent with monatomic height, (the diameter of Pt is 2.38 Å). The steps cross at *ca.* 60°, such that the terraces so formed are triangular in shape, as expected for a surface with threefold symmetry.

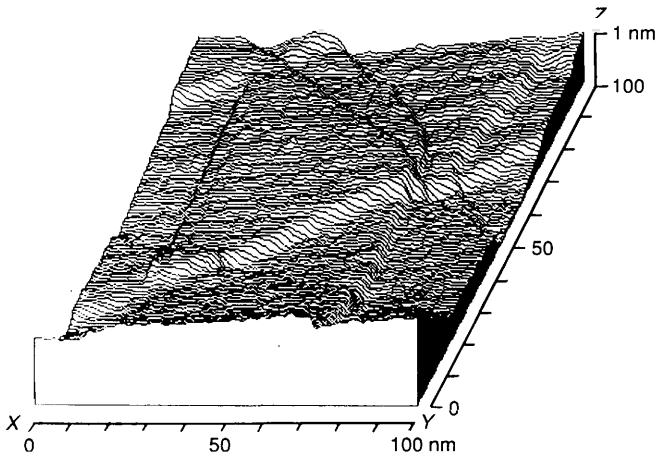

Figure 9 STM image of a 100 nm × 100 nm Pt(111) facet surface obtained in 0.5 M H_2SO_4. The electrode potentials of the Pt sample and Pt tip electrodes were 0.95 V and 0.9 V, respectively. The tunnelling current was 2 nA. Scan speed was 200 nm/s.
(With the permission of Professor K. Itaya and the *Journal of Vacuum Science and Technology*, taken from K. Itaya, S. Sugawara, K. Sashikata, and N. Furuya, *J. Vac. Sci. Technol.*, 1990, **A8**, 515.)

Figure 10 shows an image of a 1000 Å × 1000 Å area of the surface collected at 0.95 V after five potential cycles between 1.5 V and 0.05 V. After one potential cycle, noisy signals appeared on the terraces; although even after 5 cycles, the original monatomic steps can still clearly be distinguished, and the position of these steps remain unchanged. This observation is very important as it indicates that the only change induced by the potential cycling is the formation of the disordered structures on the terraces. From Figure 10, it can be seen that the disordered structures on the terraces are *randomly oriented* islands, *ca.* 30—50 Å in diameter, and one or two atoms high.

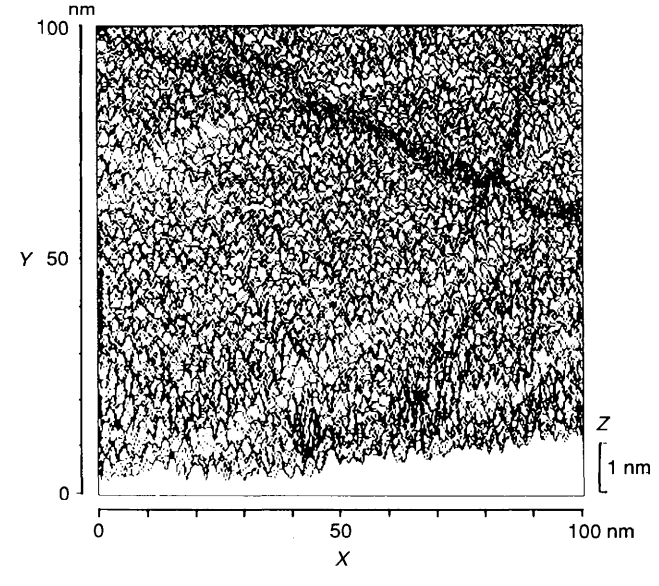

Figure 10 STM image of a 100 nm × 100 nm area of the Pt(111) surface obtained after 5 potential cycles between 1.5 V and 0.05 V. The conditions were as in Figure 9.
(With the permission of Professor K. Itaya and the *Journal of Vacuum Science and Technology*, taken from K. Itaya, S. Sugawara, K. Sashikata, and N. Furuya, *J. Vac. Sci Technol.*, 1990, **A8**, 515)

The authors observed that neither the location of the steps nor the disordered structures on the terraces changed with time in the absence of further potential cycling. However, they did observe that an image collected at 1.5 V (*i.e.* well into the region where the surface is covered with oxide) during the first cycle shows no differences from that in Figure 9, strongly suggesting that it is the *reduction* of this oxide surface, rather than its formation, that produces the structures observed in Figure 10.

The authors noted that the islands formed on the terraces are only one or two atoms high, strongly suggesting that formation of the oxide is accompanied by place-exchange, see Figure 11. Hence, they concluded that the roughening of the Pt(111) surface is *via* this place-exchange mechanism: once the oxide layer is stripped off, the Pt atoms left behind as a result of the place-exchange (in the form of adatoms) do not go back into their original positions, and this results in the observed topographical changes. It does not seem unreasonable to correlate the formation of these randomly-oriented small islands with the appearance of the polycrystalline platinum electrochemistry.

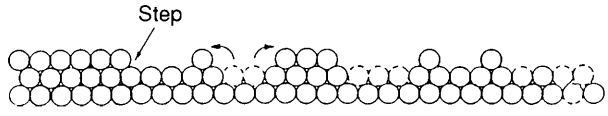

Figure 11 Schematic representation of island formation on a Pt(111) surface, induced by electrochemical cycling.

The 'eyewitness' nature of the work of Itaya and colleagues speaks volumes for the potential of STM in electrochemistry.

3 Scanning Tunnelling Spectroscopy

The images obtained in STM are often strongly dependent upon the magnitude and sign of the bias voltage, as indicated by equation 8. Equation 8 assumes that $D_s(E_{F,s})$ and $D_t(E_{F,t})$ are uniform across the surface. As was discussed above, this is a reasonable approximation for a clean metal surface (hence the tip density of states can be regarded as spatially independent).

However, for a metal upon which is an adsorbate, or for non-metals, D_s may show a marked spatial variation. As a simple example of this, consider Figure 12a, which shows a homogeneous metal surface having constant density of sites, except for the presence of a single impurity atom. Let the alien atom be more electronegative than its neighbours, such that the energy diagram at the alien atom resembles that shown in Figure 12b. If the surface is scanned in constant current mode, at a bias potential between V_{b1} and V_{b2}, (see Figure 12b), then the trajectory followed by the tip will be as shown in Figure 12a. On passing over the alien atom, the tunnelling current from the tip will be reduced, and so the feedback loop will have to move the tip closer to the surface to maintain the current. Hence, electronic information has been mixed in with the topography. The presence of the alien atom could be verified by holding the tip at a constant height above the surface, ramping the bias potential, and monitoring the tunnelling current. For locations other than that over the alien atom, we may expect a smooth increase in i_t with bias potential, (for a homogeneous and uniform density of states). However, over the alien atom, this smooth increase will have a ripple superimposed upon it where the tunnelling current is reduced due to the filled LDOS, see Figure 12c. Thus, as far as STM is concerned, it is essential when imaging electronically inhomogeneous surfaces to separate electronic from topographic effects. Fortunately, as was mentioned above, for STM on clean metal surfaces the STM image is a fairly close reflection of the surface topography. However, the surface of a semiconductor may be totally different, as a given wavefunction is often preferentially localized on specific atoms or bonds. As a result, in order to understand STM images of a semiconductor, a detailed understanding of the surface electronic structure is required.

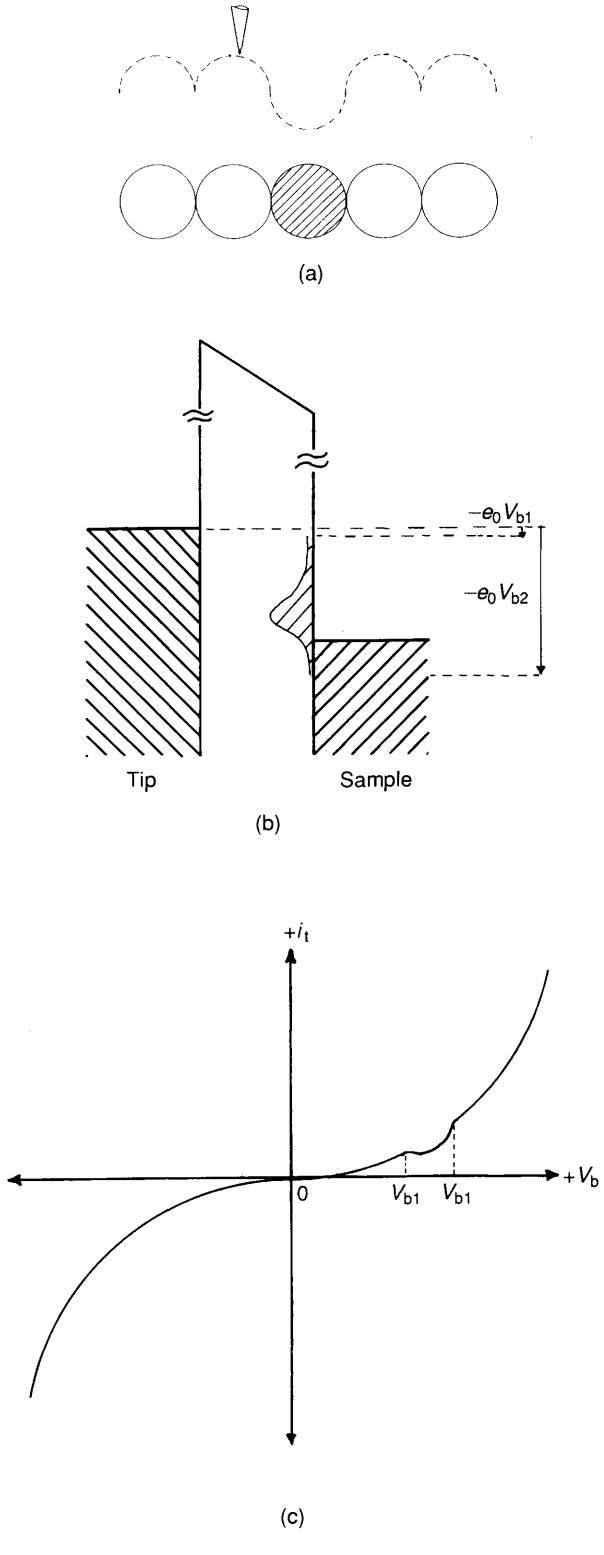

Figure 12 (a) Schematic representation of the trajectory followed by an STM tip in constant current mode over a metal sample. The surface has one alien atom, more electronegative than its neighbours. (b) Energy level diagram corresponding to case in Figure 12a. (c) A schematic representation of the STS spectrum expected if tip is poised over alien atom depicted in Figure 12a.

STS is a means of mapping out the surface electronic structure with atomic resolution. As we have seen, (Figure 4e), the LDOS of non-metal surface need not be constant. As tunnelling passes through the LDOS in Figure 4e, the tunnelling current increases or decreases slightly; this 'ripple' in the current is due to the tunnelling passing through the states comprising the LDOS and is superimposed upon the increasing background described above. This is the basis for Scanning Tunnelling Spectroscopy; the measurement of i_t *versus* V_b at fixed lateral and vertical position. In practice, in order to be able to clearly identify the energy of the 'onset' of these ripples (and hence the energies of the various states comprising the LDOS) the i/V plot is generally differentiated and the spectrum is thus presented as di_t/dV_b *versus* V_b.

In order to obtain as much information as possible, V_b should be ramped between the widest possible limits; consequently, the majority of STS studies so far reported have been performed under UHV conditions, or in air [reference 7, and references therein]. However, useful data can still be obtained in electrolyte solutions, as will be seen below.

There are essentially four common approaches to STS reported in the literature. Of these, Atom Selective Imaging,[16] Tunnelling Spectroscopy,[17] and Current Imaging Tunnelling Spectroscopy (CITS)[18] have only been reported under UHV conditions, and so will not be discussed here. The forms of Tunnelling Spectroscopy that have been employed *in situ* are simple variations of the above techniques. Tomita, Matsuda, and Itaya [see, for example, reference 19 and references therein] have employed STS *in situ* to the study of ZnO, Si, and TiO_2 in aqueous solution. The initial experiments on ZnO and TiO_2 involved monitoring the potential applied to the z-piezo, (*i.e.* the movement of the tip in the z-direction), as the bias potential was ramped at constant tunnelling current. The study on p- and n-Si(100) single-crystal electrodes[19] involved the more conventional method of monitoring i_t as a function of V_b at a constant tip–sample separation. The tip and sample potentials were controlled separately with respect to a SCE electrode *via* a bipotentiostat. Thus, Figure 13 shows the variation in the tunnelling current as the electrode potential of the n-Si sample was ramped between − 0.5 V and 0.4 V *versus* SCE; the tip potential was maintained at 0.45 V *versus* the reference, *i.e.* in the double layer region of the platinum tip. As can be seen from the plot, the tunnelling current decreased as the potential on the sample was increased, but did not fall off to zero near the flat band potential, E_{FB}, of the n-Si, as would be expected in the absence of any surface states. The shape of the plot was explained by the authors in terms of the existence of surface states. Thus, Figures 14a to c show schematic representations of the tunnelling process from sample to tip, ($E_t > E_s$), for the cases where (a) $E_s < E_{FB}$, (b) $E_s = E_{FB}$, and (c) $E_s > E_{FB}$, at constant tip potential; in the presence of surface states. In Figure 14a, tunnelling can occur from both the conduction band and the surface states; in Figure 14b, tunnelling can occur from all of the surface states. However, any surface states can only be populated up to a maximum energy less than or equal to the Fermi level and, as can be seen from Figure 14c, as the potential on the sample increases fewer states are populated; but the surface states are filled with electrons from the conduction band, hence the observed plateau in the tunnelling current. Once the Fermi level energy is lower than the lower limit of the surface state energy, the tunnelling current decreases to zero as E_s is increased to E_t. In the absence of such states, tunnelling could only occur when $E_s > E_{FB}$, (see Figure 14a). The authors commented that extending the range of V_b, by moving the tip potential to more cathodic values, would require the use of non-aqueous solvents owing to problems with hydrogen evolution at the tip.

4 Atom Force Microscopy

4.1 Introduction

The enormous success of STM has encouraged the development of a wide range of high resolution probes sensitive to force, ion

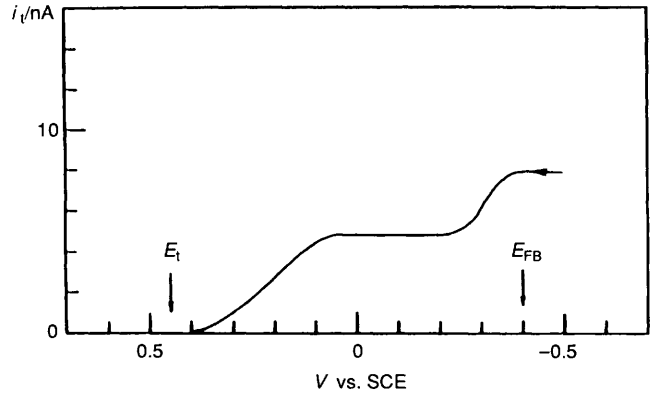

Figure 13 Tunnelling current *versus* electrode potential of n-Si at fixed tip–sample separation. The electrode potential of the tip was 0.45 V *versus* the saturated calomel electrode (SCE). The electrode potential of the silicon was scanned from − 0.5 V *versus* SCE, at a scan rate of 1 $V\,s^{-1}$.
(With the permission of Professor K. Itaya and the *Journal of Vacuum Science and Technology*, taken from E. Tomita, N. Matsuda, and K. Itaya, *J. Vac. Sci. Technol.*, 1990, **A8**, 534.)

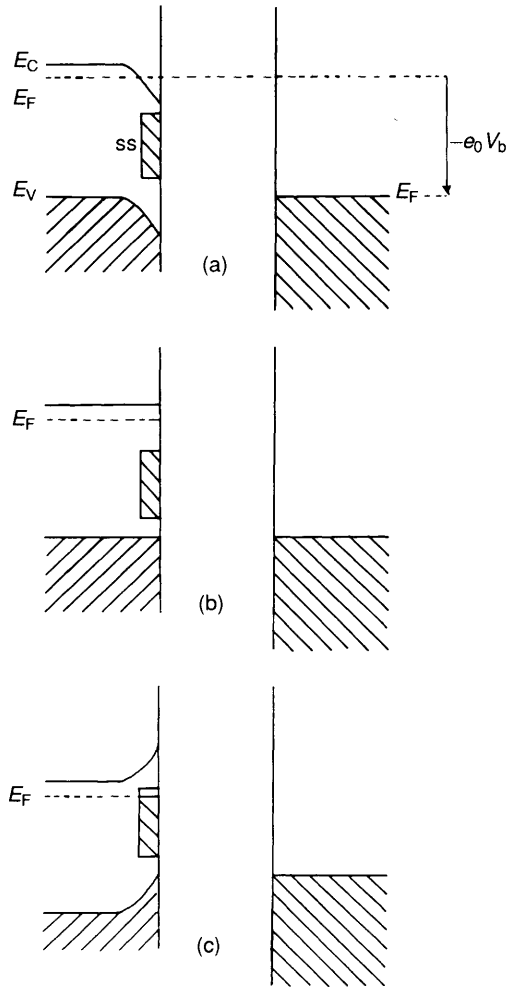

Figure 14 Schematic representations of the tunnelling process from an n-type semiconductor sample to the tip, for the cases where: (a) the sample potential, E_s, is less than the flat band potential, E_{FB}, (b) $E_s = E_{FB}$, and (c) $E_s > E_{FB}$. The tip potential is constant and the semiconductor has surface states (SS on the figure).

flow, magnetic fields, capacitance *etc.* The resolution of these probes varies according to the property measured and the size of the probe. In STM, the atomic resolution is a result of the exponential dependence of the tunnelling current on the tip–sample separation, and the consequent selection of one or two atoms on the tip for tunnelling. The atomic resolution of Atom Force Microscopy, AFM, is a result of the same form of selection, due to the inverse power law dependence of force on distance. In contrast, the magnetic force sensor depends upon several thousand magnetic moments in the tip to give measurable force; as a result, the resolution of such approaches is limited to several hundred Å.

The most common force microscopy so far employed is AFM, and it is this approach that we will concentrate upon. AFM was first reported by Binnig, Quate, and Gerber in 1986[20] and senses the van der Waals forces between the tip and sample; as a result, this technique does not require either the tip or sample to be conducting.

The dispersion forces between two bodies a distance R apart are most commonly described by the differentiated form of the Lennard–Jones potential:

$$\boldsymbol{F}(\boldsymbol{R}) = [(12C_1/R^{13}) - (6C_2/R^7)].\boldsymbol{R}(\boldsymbol{R}), \qquad (10)$$

where C_1 and C_2 are constants and $\boldsymbol{R}(\boldsymbol{R})$ is the unit vector in the R direction. The second term in equation 10 describes the long range attractive force, and the first term is the short-range repulsion experienced when the electron clouds on two atoms come into contact.

AFM has been used to image surfaces UHV,[21] under liquid,[22] and, more recently, in an electrochemical cell with the electrode under potentiostatic control.[23]

4.2 Mechanics

The exact approach employed depends upon whether the attractive or repulsive forces between tip and sample are to be probed. In both attractive and repulsive AFM, the tip is mounted on a cantilever spring, see Figure 15, with the amplitude or frequency of the spring deflection being used to obtain the surface topography as the tip is rastered across the surface. The tip is either in direct contact with the sample, (repulsive mode), or maintained above the sample, (attractive mode). In general, in both modes, the sample is moved rather than the delicate tip mount.

In attractive AFM, the tip is poised above the sample, and the cantilever vibrated using a piezocrystal. The fine (x,y,z) movement of the sample is achieved by mounting the sample on a piezo-electric stage. The tip is then vibrated by a second piezocrystal at an imposed frequency near resonance, and with an amplitude of *ca.* 20 Å. This large vibration amplitude requires a correspondingly large tip/sample separation, and in consequence leads to the reduced lateral resolution of this approach. The attractive force experienced by the tip is detected as the force gradient, $d\boldsymbol{F}(\boldsymbol{R})/dR$, which is given by:[24]

$$d\boldsymbol{F}(\boldsymbol{R})/dR = \Delta\nu/[\nu_R/2k] \qquad (11)$$

where $\Delta\nu$ is the change in vibration frequency caused by the attractive force, ν_R is the resonance frequency of the spring, and k is the spring constant of the cantilever. $\Delta\nu$ is measured *via* the determination of the change in amplitude of vibration as the tip is rastered across the surface. The image is then a plot of force *versus* lateral position.

In the repulsive mode of operation, the tip is in actual contact with the surface. An image can then be obtained in one of two principal ways; in the simplest approach, the sample is moved beneath the tip, exactly as in a record-player, the vertical deflection of the tip following directly the corrugation of the surface. This method has the great advantage of being simple, and therefore potentially cheap. The second approach involves vibrating the tip, which is still in contact with the sample, at a

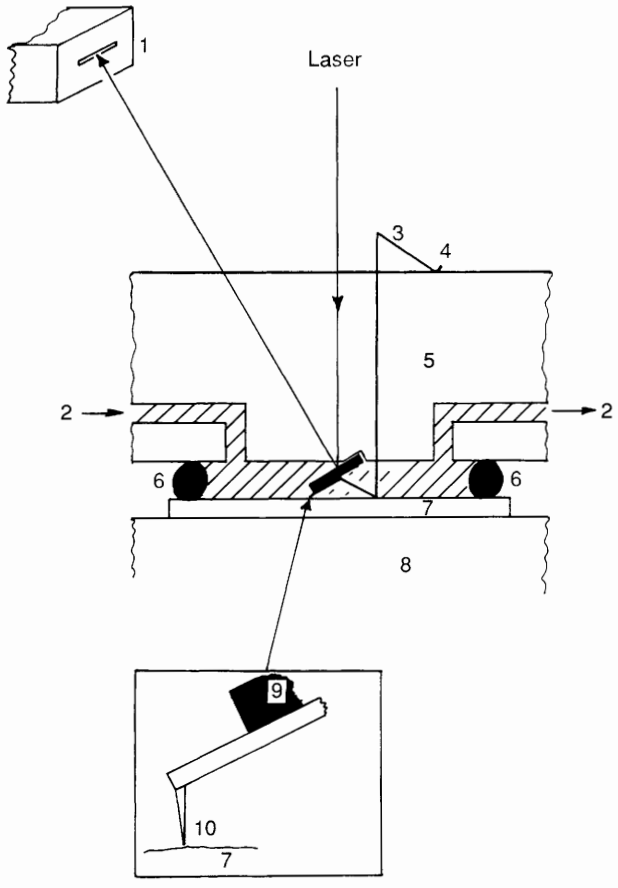

Figure 15 Schematic representation of an AFM electrochemical cell. (1) photodiode, (2) electrolyte solution inlet/outlet, (3) spring clip, (4) cantilever holder, (5) glass cell body, (6) 'O' ring, (7) sample, (8) x,y,z translator, (9) mirror, (10) tip.

frequency of several hundred Hz and an amplitude at the tip of 5—20 Å, the exact conditions depending upon the resonance frequency and spring constant of the cantilever. The amplitude of vibration is reduced on contact with the sample, this reduction being proportional to the corrugation of the surface. Profiling is achieved by moving the sample up or down during a scan to maintain a constant vibration amplitude; the image is then simply a contour map of (x,y,z), and AFM should not, in theory, suffer from the interpretational difficulties experienced in STM.

4.3 Practicalities

The original method of detecting the deflection of the tip in the early (repulsive) AFM experiments, was *via* a STM tip mounted behind the AFM tip, the latter having a metal contact on the rear of the cantilever. By applying a bias voltage across the two, the tunnelling current can then be used to determine the vertical displacement of the AFM tip. This is rather a complicated approach; in essence, all that is actually required is a means of producing, and monitoring, a signal that varies rapidly with the movement of the AFM tip. More recent approaches commonly employ optical techniques, the most simple of these involves measuring the deflection of a laser beam from a mirror mounted on the cantilever spring. The deflection is monitored by a position-sensitive detector (see Figure 15).

The use of optical techniques as the means of monitoring spring deflection has several advantages, including the fact that photons impose only a tiny force upon the tip for transmission to the sample. This has allowed AFM to be used non-destructively to image adsorbed organics, for which the force exerted on the sample must be $\leqslant 10^{-11}$ N.

It is known that the amplitude, A, of a vibration induced in a spring in response to an imposed vibration of amplitude A_0, and frequency ν_0, is:

$$A = A_0[\nu/\nu_0]^2 \tag{12}$$

where the resonance frequency of the cantilever is given by:

$$\nu_R = \sqrt{[k/m]}, \tag{13}$$

where m is the mass of the spring. Thus, in order for the vibrational noise on the tip to be as low as possible, ν_R must be as high as possible; in turn, this indicates that the mass of the spring should be low. Tips with high resonance frequencies are now commercially available.

Typically, a building vibration has $A_0 \sim 1\mu$m and $\nu = 20$ Hz; for a common cantilever spring resonance frequency of 10 kHz, this gives a noise amplitude of 0.04 Å. This will cause very little interference and, as a result, atomic resolution is possible with very little vibrational isolation, in complete contrast to STM.

4.3.1 The Underpotential Deposition of Copper on Gold(111)

Underpotential deposition (upd) is a much-studied phenomenon in electrochemistry, and is the electrochemical reduction of a metal cation to form a monolayer or submonolayer of the corresponding metal at the surface of an electrode. The critical point is that deposition occurs at a potential higher than that dictated by the reversible potential of the metal/metal cation couple, suggesting that such a upd layer is energetically quite different from the bulk metal. However, subsequent deposition on a upd monolayer occurs at the expected potential and the resulting surface is typical of the bulk metal.

The upd process at noble metal surfaces is of considerable interest for several reasons: (i) as a model of deposition in general; (ii) upd surfaces show increased resistance to poisoning by oxidation products and thus are of interest with respect to fuel cell and biosensor development; (iii) the distinctive chemical properties of the upd surface.

A representative example of the upd process is copper on gold and an extremely illuminating study upon this system using repulsive AFM was reported by Manne, Hansma, Massie, Elings, and Gewirth.[23] The authors employed a commercially available AFM, the essentials of which are shown in Figure 15. The reference electrode was a copper wire in contact with the electrolyte at the outlet of the cell. The counter electrode was the stainless steel spring clip holding the AFM cantilever in place. The working electrode was a 100 nm-thick evaporated Au film [which is known to expose mainly the Au(111) surface] mounted upon an (x,y) translator.

Figure 16 shows the Au(111) surface in 0.1 M $HClO_4$/ 1×10^{-3} M $CuClO_4$ at + 0.7 V, prior to the deposition of the Cu. The (x,y) displacement of the translator was calibrated using the known atom–atom spacing of the close-packed Au(111) lattice of 2.9 Å. The image was the same when 0.1 M H_2SO_4/ 1×10^{-3} M $CuSO_4$ was employed as the electrolyte; a surprising observation in the light of the fact that SO_4^{2-} is thought to be strongly adsorbed at this potential. The authors postulated that either sulfate is not as strongly adsorbed as was previously thought, or the AFM tip 'pushes away' the adsorbed SO_4^{2-} during its passage across the surface.

Figure 17 shows an image collected at − 0.1 V in the perchlorate solution after the bulk deposition of several monolayers of Cu. The Cu–Cu distance in the figure was found to be 2.6 Å, which was taken as evidence of the Cu atoms simply sitting 'on top' of the underlying gold atoms. Sweeping the potential up to + 0.11 V stripped off all but the initially deposited upd layer. At this point, the authors observed that the nature of the electrolyte had a major effect upon the structure of the adsorbed Cu. Thus, Figure 18a shows a schematic representation Au(111)/upd Cu surface in the perchlorate electrolyte. The Cu–Cu spacing was the same as for the Au(111) surface at 0.7 V, 2.9 Å. The Cu

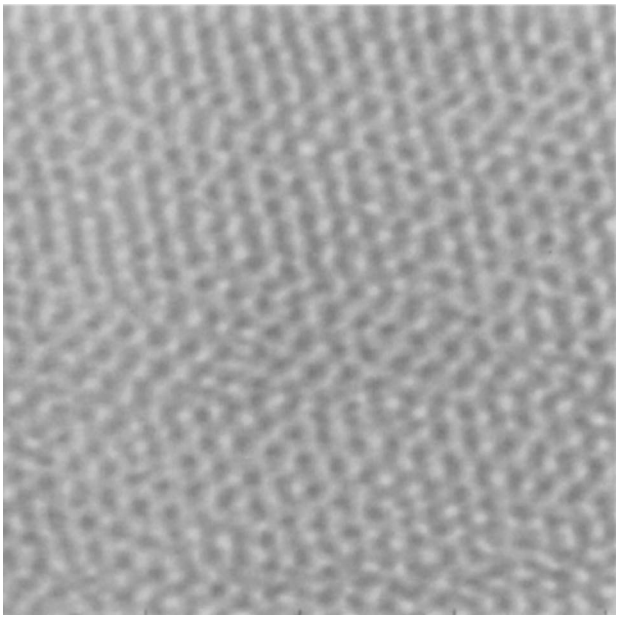

Figure 16 AFM image of the Au(111) surface in 0.1 M $HClO_4$/1 × 10^{-3} M $CuClO_4$ at 0.7 V, prior to copper deposition. The reference electrode was a copper wire in contact with the same electrolyte. The Au–Au spacing is 2.9 Å.
(By permission of Professor A. Gewirth and Science, taken from S. Manne, P. K. Hansma, J. Massie, V. B. Elings, and A. A. Gewirth, *Science*, 1991, **251**, 185. Copyright 1991 by the AAAS).

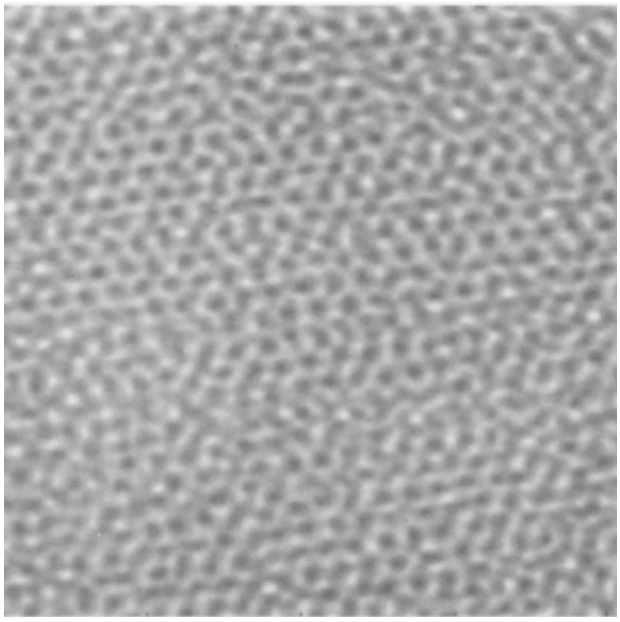

Figure 17 AFM image of Au(111) surface after bulk deposition of several monolayers of Cu. The potential of the gold is − 0.1 V, and Cu–Cu spacing is 2.6 Å.

lattice, however, was no longer exactly overlying, *i.e.* commensurate with the underlying gold lattice. It appeared that the Cu lattice direction was rotated by 30° ± 10° relative to the gold. The authors attributed this re-arrangement to the strain of incorporating the larger copper atoms into a close-packed structure exactly over the Au(111) surface (Cu radius 1.75 Å, Au 1.42 Å). In 0.1 M H_2SO_4 at + 0.144 V, the upd Cu layer formed a much more open lattice (see Figure 18b) with a Cu–Cu spacing of 4.9 Å; an observation supported by STM.[24] The authors postulated that the more open structure found in the sulfuric acid electrolyte was due to the stabilization of the Cu monolayer by co-adsorption with SO_4^{2-}, although they had not observed this co-adsorbed sulfate directly. This was supported by radiochemical data which showed that, prior to Cu upd on gold, there is little or no sulfate on the gold surface. Immediately following the deposition, substantial sulfate adsorption occurs.

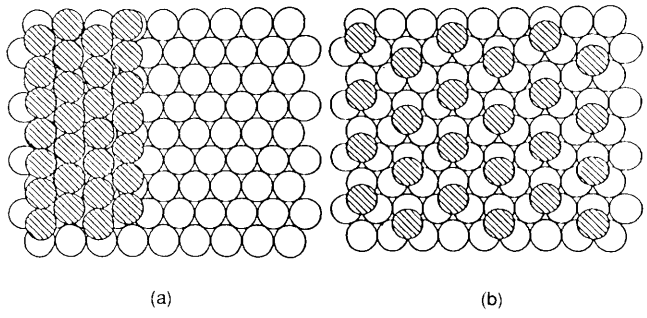

Figure 18 (a) Schematic representation of the incommensurate close-packed overlayer of Cu on Au formed in the perchlorate electrolyte. The open circles are the gold atoms. Only part of the monolayer is shown in order to exhibit the overlayer–underlayer orientation. (b) Schematic representation of the more open lattice formed in the sulfuric acid electrolyte.

On sweeping the potential back to + 0.7 V, the upd Cu was removed and the original Au(111) surface regained, showing unequivocally that the upd of Cu on Au(111) in either electrolyte is completely reversible, contrary to some previous speculation.

Thus, AFM is a very powerful complement to STM and has the great advantage of not involving quantum-mechanical tunnelling. This means that non-conducting samples can be imaged, both in terms of the surface and any adsorbate, and that images can be obtained when Faradaic current is flowing, as in the study discussed above. The latter could not be done with STM, as a Faradaic current can have a disastrous effect upon the tunnelling current. Hence AFM offers the very real possibility of real-time imaging, and is certain to become an important *in situ* tool of the future in electrochemistry.

Acknowledgements. I would like to thank Professor A. Hamnett for helpful consultations, and both he and Mr J. Brooker for critical appraisal of the manuscript.

5 References

1 'Comprehensive Chemical Kinetics', ed., R. G. Compton and A. Hamnett, Elsevier, Amsterdam, Vol. 29, 1989.
2 'Spectroelectrochemistry: Theory and Practice', ed. R. J. Gale, Plenum Press, New York, 1988.
3 G. Binnig, H. Rohrer, Ch. Gerber, and E. Weibel, *Phys. Rev. Lett.*, 1982, **49**, 57.
4 T. R. I. Cataldi and G. A. D. Briggs, personal communication.
5 R. Sonnenfeld, J. Schneir, and P. K. Hansma, 'Modern Aspects of Electrochemistry', ed. R. E. White, J. O'M. Bockris, and B. E. Conway, Plenum Press, New York, 1990, p. 1.
6 T. R. I. Cataldi, I. G. Blackham, G. A. D. Briggs, J. Pethica, and H. A. O. Hill, *J. Electroanal. Chem.*, 1990, **290**, 1.
7 (*a*) R. J. Hamers, *Ann. Rev. Phys. Chem.*, 1989, **40**, 531; (*b*) 'Scanning Tunnelling Microscopy and Related Methods', ed. R. J. Behm, N. Garcia and H. Rohrer, NATO ASI Series, Series E: Applied Sciences Vol 184, Kluwer Academic Publishers, Dordrecht, 1990.
8 J. V. Coe, G. H. Lee, J. G. Eaton, S. T. Arnold, H. W. Sarkas, K. H. Bowen, C. Ludewigt, H. Haberland, and D. Worsnop, *J. Chem. Phys.*, 1990, **92**, 3980.
9 W. Haiss, D. Lackey, J. K. Sass, and K. H. Besocke, *J. Chem. Phys.*, in press.
10 R. Sonnenfeld and P. K. Hansma, *Science*, 1986, **232**, 211.
11 F.-R. Fan and A. J. Bard, *J. Electrochem. Soc.*, 1989, **136**, 3216.
12 R. Christoph, H. Siegenthaler, H. Rohrer, and H. Wiese, *Electrochim. Acta*, 1989, **34**, 1011.

13 D. J. Trevor, C. E. D. Chidsey, and D. N. Loiacono, *Phys. Rev. Lett.*, 1989, **62**, 929.
14 H. Honbo and K. Itaya, *Nouv. J. Chim.*, in press.
15 K. Itaya, S. Sugawara, K. Sashikata, and N. Furuya, *J. Vac. Sci. Technol.*, 1990, **A8**, 515.
16 R. M. Feenstra, J. A. Stroscio, J. Tersoff, and A. P. Fein, *Phys. Rev. Lett.*, 1987, **58**, 1192.
17 R. S. Becker, J. A. Golovchenko, D. R. Hamann, and B. S. Swartzentruber, *Phys. Rev. Lett.*, 1985, **55**, 2032.
18 R. J. Hamers, R. M. Tromp, and J. E. Demuth, *Phys. Rev. Lett.*, 1986, **56**, 1972.
19 E. Tomita, N. Matsuda, and K. Itaya, *J. Vac. Sci. Technol.*, 1990, **A8**, 534.
20 G. Binnig, C. F. Quate, and Ch. Gerber, *Phys. Rev. Lett.*, 1986, **12**, 930.
21 J. A. Stroscio, R. M. Feenstra, and A. P. Fein, *Phys. Rev. Lett.*, 1987, **58**, 1668.
22 O. Marti, B. Drake, and P. K. Hansma, *Appl. Phys. Lett.*, 1987, **51**, 484.
23 S. Manne, P. K. Hansma, J. Massie, V. B. Elings, and A. A. Gewirth, *Science*, 1991, **251**, 183.
24 O. M. Magnussen, J. Hotlos, R. J. Nichols, D. M. Kolb, and R. J. Behm, *Phys. Rev. Lett.*, 1990, **64**, 2929.
25 P. K. Hansma, V. B. Elings, O. Marti, and C. E. Bracker, *Science*, 1988, **242**, 209.